TRENDS IN SCIENCES 2026; 23(10): 13136
https://doi.org/10.48048/tis.2026.13136 RESEARCH ARTICLE

Geraniin-Rich Rambutan Peel Nanoemulsion: Enzyme Inhibition and Antioxidant Activities for Cosmeceutical Applications

Panita Kongsune[1,2], Parichat Thepthong[1,2], Khwanchanok Matpoom[1,2], Wilasinee Langmuang[1], Luksika Kongjun[3] and Netnapa Chana[2,4,*]

[1]Department of Chemistry, Faculty of Science and Digital Innovation, Thaksin University, Phatthalung Campus, Phatthalung 93210, Thailand
[2]Innovative Material Chemistry for Environment Center, Department of Chemistry, Faculty of Science and Digital Innovation, Thaksin University, Phatthalung campus, Phatthalung 93210, Thailand
[3]Thaksin University Demonstration School, Phatthalung Campus, Phatthalung 93210, Thailand
[4]Department of Biotechnology, Faculty of Science and Digital Innovation, Thaksin University, Phatthalung Campus, Phatthalung 93210, Thailand

([*]Corresponding author's e-mail: netnapa@tsu.ac.th)

Received: 23 December 2025, Revised: 28 March 2026, Accepted: 10 April 2026, Published: 25 May 2026

Abstract

This study evaluated the anti-aging potential of rambutan (*Nephelium lappaceum* L.) peel extract through phytochemical profiling, enzyme inhibition, molecular docking, and nanoemulsion formulation. The extract showed high phenolic content and strong antioxidant activity (DPPH IC_{50} = 3.53 ± 0.05 µg/mL). LC-MS/MS analysis identified geraniin and ellagic acid as major bioactive compounds. The extract exhibited concentration-dependent inhibition of key skin-aging enzymes, with pronounced collagenase inhibition and moderate elastase and tyrosinase inhibition, supported by molecular docking demonstrating strong binding affinity of geraniin. Optimized oil-in-water nanoemulsions displayed nanoscale particle sizes (266.7 - 275.5 nm) with moderate polydispersity (PDI = 0.325 - 0.332) and excellent physicochemical stability over 7 days. Notably, the nanoemulsion system enhanced the stability and functional delivery of phenolic compounds, providing a practical approach for improving bioactivity in cosmeceutical formulations while promoting the valorization of rambutan peel waste within a circular economy framework. The formulations retained high antioxidant activity (91% - 95%), tyrosinase inhibition, and antibacterial activity against *Staphylococcus aureus*. These results demonstrate the potential of geraniin-rich rambutan peel nanoemulsions as promising candidates for cosmeceutical applications.

Keywords: Anti-aging, Enzyme inhibition, Molecular docking, Nanoemulsion, Rambutan peel

Introduction

Skin aging is a complex biological process characterized by progressive deterioration of structural and functional integrity, manifesting as wrinkles, loss of elasticity, and hyperpigmentation. This multifactorial phenomenon involves intrinsic aging driven by chronological time and cellular senescence, as well as extrinsic aging accelerated by environmental stressors such as ultraviolet radiation, pollution, and lifestyle factors [1]. At the molecular level, excessive production of reactive oxygen species (ROS) leads to oxidative damage of proteins, lipids, and DNA [2]. Concurrently, matrix metalloproteinases (MMPs), particularly collagenase (MMP-1) and elastase, are upregulated, resulting in degradation of collagen and elastin within the dermal extracellular matrix [3], while tyrosinase overactivity contributes to hyperpigmentation and photoaging [4].

To counteract these mechanisms, synthetic agents such as retinoids, hydroquinone, and kojic acid have

been widely used; however, concerns regarding irritation and long-term safety have increased interest in natural alternatives. Plant-derived polyphenols have attracted significant attention due to their antioxidant, enzyme inhibitory, and anti-inflammatory activities, although comprehensive safety evaluations remain limited [5-7]. In parallel, circular economy approaches have emphasized the valorization of agricultural by-products into high-value applications.

Rambutan (*Nephelium lappaceum* L.) peel, a major agro-industrial waste, is a rich source of phenolic compounds, including ellagitannins such as geraniin and corilagin, as well as ellagic acid and flavonoids [8,9]. Reported total phenolic content varies depending on extraction methods, with advanced techniques such as ultrasound-assisted extraction significantly enhancing phenolic recovery [10,11], while enriched fractions can achieve substantially higher values [12]. Rambutan peel has demonstrated promising anti-aging activities, including anti-melanogenesis, tyrosinase inhibition, and stimulation of collagen-related pathways [14,15]. However, its practical application in cosmeceutical formulations remains limited due to poor aqueous compatibility, instability, and formulation-related constraints affecting bioavailability [16].

Nanoemulsion systems offer an effective strategy to overcome these limitations by improving solubility, stability, and delivery of bioactive compounds through nanoscale dispersion [17,18]. Additionally, certain plant polyphenols may contribute to emulsion stabilization via interfacial and rheological modifications [19]. Molecular docking analysis further provides mechanistic insights into enzyme–inhibitor interactions, supporting experimental findings in anti-aging research [20,21].

Despite these advances, integrative studies combining phytochemical profiling, multi-enzyme inhibition, molecular docking, and nanoemulsion formulation with stability evaluation for rambutan peel extracts remain limited. In particular, the development of stable nanoemulsion systems incorporating rambutan peel extract for cosmeceutical applications has not been systematically investigated. Therefore, this study aims to address these gaps by integrating experimental and computational approaches to evaluate antioxidant and anti-aging enzyme inhibitory activities, elucidate enzyme–inhibitor interactions, and develop stable nanoemulsion formulations, contributing to sustainable agricultural waste valorization and cosmeceutical development.

Materials and methods

Chemicals

Enzymes and substrates: Porcine pancreatic elastase (Type I), collagenase Type V, mushroom tyrosinase, N-Succinyl-Ala-Ala-Ala-*p*-nitroanilide (elastase substrate), P-z peptide (collagenase substrate), and L-3,4-dihydroxyphenylalanine (L-DOPA) (tyrosinase substrate) were purchased from Sigma-Aldrich (St. Louis, MO, USA). Standard compounds and reagents, including (-)-epigallocatechin gallate (EGCG, ≥ 95%), kojic acid, ascorbic acid, 2,2-diphenyl-1-picrylhydrazyl (DPPH), 2,2'-azino-bis(3-ethylbenzothiazoline-6-sulfonic acid) diammonium salt (ABTS), 2,4,6-tris(2-pyridyl)-*s*-triazine (TPTZ), Folin-Ciocalteu reagent, and gallic acid, were also obtained from Sigma-Aldrich (St. Louis, MO, USA). All other chemicals were of analytical grade.

Plant material and extraction

Fresh rambutan fruits (*Nephelium lappaceum* Linn. cv. Rong Rien) with red spines were obtained from a local market in Pa Phayom District, Phatthalung Province, Thailand, within 24 h post-harvest. Fruits at commercial maturity were selected based on uniform size and intact peel condition. The peels were manually separated, washed with distilled water, and air-dried at room temperature for 24 h, followed by oven-drying at 50 °C for 24 h until the moisture content reached below 5%. The dried peels were ground into fine powder using a mechanical grinder and stored at −20 °C in sealed containers until use.

Ultrasonic-assisted extraction was performed using an ultrasonic bath (40 kHz, 150 W; Elma Schmidbauer, Singen, Germany). Dried peel powder (300 g) was extracted with 95% ethanol (1,500 mL; solid-to-solvent ratio 1:5, w/v) for 30 min at controlled temperature (below 40 °C). The selection of 95% ethanol was based on its intermediate polarity suitable for phenolic extraction [22], while the 30-min extraction duration was adopted from previous ultrasonication studies demonstrating optimal phenolic recovery within this timeframe [23,24]. Bath temperature was monitored and maintained below 40 °C throughout extraction to

minimize thermal degradation of phenolic compounds [23]. The extract was filtered through Whatman No. 1 filter paper and concentrated using a rotary evaporator (Buchi Labortechnik AG, Flawil, Switzerland) at 45 °C under reduced pressure. Three independent extraction batches were prepared under identical conditions. The extraction yield was 15.29 ± 1.40% (w/w, dry weight basis).

Total phenolic content analysis

Total phenolic content was determined spectrophotometrically using the Folin-Ciocalteu method as described by Kongsune *et al.* [25] with minor modifications. A gallic acid calibration curve was prepared at concentrations of 5, 10, 25, 75, 300, 500, and 750 µg/mL. The dried extract was reconstituted in 95% ethanol to a final concentration of 1 mg/mL. Sample or standard (60 µL) was mixed with 2.5 mL of 10% (v/v) Folin-Ciocalteu reagent, followed by 2 min equilibration. Subsequently, 2.0 mL of 7.5% (w/v) sodium carbonate solution was added, and the mixture was incubated in the dark at 50 °C for 15 min. Absorbance was measured at 765 nm using a UV-Vis spectrophotometer. Results were calculated from the gallic acid standard curve and expressed as milligrams of gallic acid equivalents per gram of extract (mg GAE/g extract). All determinations were performed in triplicate.

DPPH radical scavenging assay

Antioxidant capacity was evaluated using the DPPH free radical scavenging assay as described by Kongsune *et al.* [25], with minor modifications. The DPPH working solution was prepared at a concentration of 0.2 mM in methanol. The dried extract was reconstituted in 95% ethanol to 1 mg/mL, then serially diluted to obtain final concentrations ranging from 0.5 to 10 µg/mL. Sample solution (0.1 mL) was mixed with 2.9 mL of DPPH solution and incubated in the dark at room temperature for 30 min to reach reaction completion. Absorbance measurements were recorded at 517 nm using a UV-Vis spectrophotometer. Ascorbic acid was used as a positive control. The percentage of DPPH radical scavenging activity was calculated according to the following equation:

$$\text{DPPH scavenging activity (\%)} = [(A_{control} - A_{sample}) / A_{control}] \times 100$$

where $A_{control}$ represents the absorbance of the control reaction containing the DPPH solution, and A_{sample} represents the absorbance of the sample reaction with the DPPH solution. The half-maximal inhibitory concentration (IC_{50}) was determined from linear regression analysis of the concentration-response relationship data. All measurements were performed in triplicate.

ABTS radical cation decolorization assay

Antioxidant capacity was assessed using the ABTS radical cation decolorization assay as described by Re *et al.* [26]. The ABTS radical cation ($ABTS^{\bullet+}$) was generated by mixing 7 mM ABTS stock solution with 2.45 mM potassium persulfate in equal volumes and incubating the mixture in the dark at room temperature for 12 - 16 h. The $ABTS^{\bullet+}$ working solution was prepared by diluting the stock solution with methanol to achieve an absorbance of 0.70 ± 0.02 at 734 nm. The dried extract was reconstituted in 95% ethanol to a concentration of 1 mg/mL and serially diluted to the desired concentration range. Sample solution (300 µL) was mixed with 2.7 mL of the $ABTS^{\bullet+}$ working solution, followed by incubation in the dark at room temperature for 30 min. Absorbance was measured at 734 nm using a UV-Vis spectrophotometer. Ascorbic acid was used as a positive control. The percentage of ABTS radical scavenging activity was calculated according to the following equation:

$$\text{ABTS scavenging activity (\%)} = [(A_{control} - A_{sample}) / A_{control}] \times 100$$

where $A_{control}$ represents the absorbance of the control reaction and A_{sample} represents the absorbance of the sample. The half-maximal inhibitory concentration (IC_{50}) was determined from linear regression analysis of the concentration-response relationship data. All measurements were performed in triplicate.

FRAP assay

The FRAP assay was performed to evaluate the reducing power of the rambutan peel extract, following the method described by Benzie and Strain [27] with slight modifications. The FRAP working reagent was

freshly prepared by mixing 300 mM acetate buffer (pH 3.6), 10 mM 2,4,6-tripyridyl-s-triazine (TPTZ) solution in 40 mM HCl, and 20 mM ferric chloride ($FeCl_3 \cdot 6H_2O$) solution in a ratio of 10:1:1 (v/v/v), respectively. The reagent was warmed to 37 °C prior to use. The extract solution (300 µL) was mixed with pre-warmed FRAP reagent (2.7 mL), and the reaction mixture was incubated at 37 °C for 30 min in the dark. Absorbance was measured at 593 nm using a UV-Vis spectrophotometer. Ferrous sulfate ($FeSO_4 \cdot 7H_2O$) was used to construct the standard calibration curve ($R^2 > 0.999$). Ferrous sulfate was used as the reference standard to quantify the reducing capacity of the extract, as it provides a reliable measure of ferric-to-ferrous ion reduction in the FRAP assay [27]. The results were expressed as micromoles of ferrous ion (Fe^{2+}) equivalents per gram of extract (µmol Fe^{2+}/ g extract). All measurements were performed in triplicate.

Tyrosinase inhibition activity

Tyrosinase inhibition activity was determined using L-DOPA as the substrate according to the method of Fan *et al*. [28] with modifications. The extract was dissolved in 10% DMSO and prepared at various concentrations. The final concentration of DMSO was kept constant in all reaction mixtures, including controls, and preliminary experiments confirmed that it did not significantly affect tyrosinase activity. This condition was consistently applied in all enzyme inhibition assays. The reaction mixture contained 50 µL of sample solution, 100 µL of L-DOPA (2 mM in 50 mM phosphate buffer, pH 6.8), and 50 µL of mushroom tyrosinase (1000 U/mL). The mixture was incubated at 37 °C for 15 min, and dopachrome formation was measured at 475 nm using a microplate reader (Thermo Fisher Scientific, Waltham, MA, USA). Kojic acid served as the positive control, while 10% DMSO was used as the negative control [29]. The substrate concentration (2 mM) was selected to ensure near-saturating conditions, based on the study of Deri *et al.* [30]. Percentage inhibition was calculated using the formula:

$$\% \text{ Inhibition} = [(A_0 - A_1)/A_0] \times 100$$

where A_0 and A_1 represent the absorbance of the control and sample, respectively. IC_{50} values, defined as the concentration required for 50% enzyme inhibition, were determined by linear regression analysis using Microsoft Excel. All assays were performed in triplicate, and results were expressed as mean ± standard deviation.

Collagenase inhibition activity

Collagenase inhibitory activity was evaluated using a colorimetric assay with P-z peptide as the substrate, according to the method of Lee *et al.* [31] with minor modifications. The extract was dissolved in DMSO to prepare stock solutions, yielding final assay concentrations of 0.001 - 1 mg/mL, and the solvent conditions were maintained as described above. Ascorbic acid was used as the positive control due to its recognized role in collagen protection and its reported inhibitory effects on collagenase activity [32]. The assay was performed in a total volume of 200 µL containing 50 µL of sample solution, 100 µL of P-z peptide substrate (1 mM in 50 mM Tricine buffer, pH 7.5, supplemented with 10 mM $CaCl_2$ and 400 mM NaCl), and 50 µL of bacterial collagenase from *Clostridium histolyticum* (0.2 U/mL). The substrate concentration (1 mM) was selected based on reported Km values (< 1 mM) to ensure near-saturating conditions [33]. Bacterial collagenase was employed as a screening model due to its reproducibility and widespread use in collagen degradation studies [34]. The reaction mixture was incubated at 37 °C for 20 min, and absorbance was measured at 320 nm using a microplate reader (Thermo Fisher Scientific, Waltham, MA, USA). Control reactions contained 10% DMSO without extract. Collagenase inhibitory activity was calculated using the following formula:

$$\% \text{ Inhibition} = [(A_0 - A_1)/A_0] \times 100$$

where A_0 represents the absorbance of the control and A_1 represents the absorbance of the sample. IC_{50} values were determined by linear regression analysis using Microsoft Excel. All experiments were performed in triplicate, and results were expressed as mean ± standard deviation.

Elastase inhibition activity

Elastase inhibitory activity was determined using N-succinyl-Ala-Ala-Ala-p-nitroanilide as substrate according to the method described by Lee *et al.* [35] with modifications. The assay mixture contained 100

mM Tris-HCl buffer (pH 8.0), porcine pancreatic elastase (0.2 U/mL), and the extract at various concentrations. The mixture was preincubated at 37 °C for 15 min, followed by the addition of the substrate (0.8 mM final concentration). The enzymatic reaction was monitored spectrophotometrically at 410 nm for 30 min at 37 °C. The release of p-nitroaniline from the substrate was measured, and elastase inhibitory activity was calculated using the following formula:

$$\% \text{ Inhibition} = [(A_0 - A_1)/A_0] \times 100$$

with A_0 = control absorbance and A_1 = sample absorbance. IC_{50} values were obtained by plotting percentage inhibition versus extract concentration. Epigallocatechin gallate (EGCG) served as the positive control. EGCG was chosen as the positive control owing to its potent elastase inhibitory activity and its extensive application as a benchmark compound in anti-aging and cosmeceutical research [36]. The substrate concentration (0.8 mM) was selected based on reported Km values (~0.88 mM) to ensure near-saturating conditions [37]. Measurements were conducted in triplicate.

LC-MS analysis

The phytochemical profile of the rambutan peel extract was characterized using liquid chromatography-quadrupole time-of-flight mass spectrometry (LC-QTOF-MS) according to the protocol previously described by Kongsune *et al.* [25]. The analysis was performed on an Agilent 1290 Infinity II LC system coupled to a 6545 Q-TOF mass spectrometer. Chromatographic separation was achieved using a Zorbax Eclipse Plus C18 column (1.8 μm, 2.1×100 mm^2) maintained at 40 °C. The mobile phase consisted of 0.1% formic acid in deionized water (Solvent A) and 0.1% formic acid in acetonitrile:water mixture (80:20, v/v) (Solvent B). The gradient elution was programmed at a constant flow rate of 0.2 mL/min as follows: 0 - 45 min, 0% - 100% B; 45 - 50 min, isocratic at 100% B; 50 - 60 min, return to initial conditions (100% A); and 60 - 65 min, re-equilibration with 100% A. Mass spectrometric detection was operated in negative electrospray ionization (ESI^-) mode. The mass scanning ranges were set at *m/z* 100 - 1,200 for MS and *m/z* 50 - 1,200 for MS/MS, utilizing collision energies of 10, 20, and 40 V. Data acquisition and compound identification were processed using Agilent MassHunter software. Compounds were tentatively identified based on accurate mass measurements, MS/MS fragmentation patterns, and database matching against the METLIN and PCDL libraries (match score > 80). Structural assignments were further supported by comparison with previously reported LC-MS-based phenolic profiling studies [38]. Major compounds were assigned based on consistent matches with literature-reported MS/MS spectra and retention behaviors. The relative abundance of individual compounds was estimated based on normalized peak area percentages derived from extracted ion chromatograms (EICs), and no external standards were employed for absolute quantification. Therefore, all compound identifications should be considered tentative unless confirmed with authentic reference standards.

Molecular docking analysis

In silico molecular docking studies were conducted to elucidate the potential binding interactions and binding energies of the identified phytochemicals against key skin-aging enzymes, namely tyrosinase, collagenase, and elastase. The crystal structures of the target enzymes were retrieved from the RCSB Protein Data Bank (PDB), with PDB IDs of 2Y9X [39], 7Z5U [40], and 1ELE [41], respectively. The 3D structures of the bioactive compounds identified from the rambutan peel extract were constructed using GaussView 5.0.8 and subsequently optimized at the Hartree–Fock (HF) level with the 6-31G basis set using Gaussian 09 [42]. For protein preparation, all crystallographic water molecules and co-crystallized ligands were removed from the PDB files to simplify the docking system. AutoDockTools (ADT) was employed to prepare the protein structures by adding polar hydrogen atoms and assigning Gasteiger charges. Molecular docking simulations were performed using AutoDock 4.2 [43] with the Lamarckian Genetic Algorithm (LGA). Docking parameters were set as follows: grid box size of 60×60×60 points with a spacing of 0.375 Å centered on the active site, and 100 independent docking runs were performed for each ligand-protein complex [39-41].

The resulting conformations were clustered using a root-mean-square deviation (RMSD) tolerance of 2.0 Å. The docking pose with the lowest binding energy within the most populated cluster was selected for subsequent analysis of binding interactions. The docking protocol was validated by redocking the crystallographic ligands into their respective binding sites, yielding RMSD values of 1.21 Å for tyrosinase, 1.47 Å for collagenase, and 1.36 Å for elastase, confirming the reliability of the docking methodology.

Explicit crystallographic water molecules were removed prior to docking in order to standardize the binding environment and improve computational efficiency, consistent with common preliminary screening workflows. Therefore, the resulting docking scores are used to compare relative binding tendencies rather than to represent absolute binding affinities, particularly for polyphenolic compounds that can involve water-mediated contacts.

Preparation and characterization of rambutan peel-loaded nanoemulsions

The nanoemulsions were prepared using the spontaneous emulsification method, which relies on the rapid diffusion of a hydrophilic surfactant and/or co-solvent from the oil phase into the aqueous phase, resulting in a significant reduction in interfacial tension and spontaneous formation of fine oil droplets without high-energy input [35]. Two non-ionic surfactant systems were employed: polyethylene glycol 400 (PEG 400)-based surfactant for the PR series and polysorbate 80 (Tween 80)-based surfactant for the TR series. For extract-loaded formulations, the rambutan peel ethanolic extract (1 mg/mL) was incorporated into the oil-surfactant phase prior to emulsification to achieve encapsulation within the lipid core. The oil phase, surfactant, and aqueous phase were mixed at predetermined volume ratios as detailed in **Table 4** to obtain a final volume of 50 mL. The mixtures were stirred at 500 rpm using a magnetic stirrer at room temperature for 30 min to ensure homogeneity. The extract was added to achieve a final concentration of 20 µg/mL, which was selected based on preliminary screening to ensure colloidal stability while maintaining measurable bioactivity and avoiding droplet destabilization caused by excessive polyphenol loading. Following extract incorporation, the formulations were homogenized at 5,000 rpm for 3 min and subsequently subjected to ultrasonication using a probe sonicator operating at 20 kHz frequency and 40% amplitude (150 W output power) for 5 min to ensure uniform dispersion of the bioactive compounds. During homogenization and ultrasonication, the sample temperature was monitored and maintained below 30 °C by placing the samples in an ice bath to prevent thermal degradation of phenolic compounds.

The particle size (Z-average diameter), polydispersity index (PDI), zeta potential, and electrical conductivity of the nanoemulsions were measured using dynamic light scattering (DLS) and electrophoretic light scattering (ELS) techniques with a Zetasizer Nano ZS (Malvern Instruments, Malvern, UK) [44]. The effects of extract incorporation on nanoemulsion properties were evaluated by comparing formulations with and without the extract. All measurements were performed in triplicate and reported as mean ± standard deviation. Physical stability was assessed by visual inspection for phase separation, color changes, and transparency over a 7-day storage period at room temperature (25 ± 2 °C). It should be noted that the 7-day stability evaluation represents a short-term assessment; therefore, further long-term studies under extended storage conditions are required to confirm the robustness and practical applicability of the developed nanoemulsion systems. Morphological examination of nanoemulsion droplets was performed using bright-field optical microscopy with an Olympus BX-51 microscope equipped with a digital camera system.

Evaluation of biological activities of rambutan peel extract-loaded nanoemulsions

Antibacterial activity

The antibacterial activity of the extract-loaded nanoemulsions was evaluated against Gram-positive *Staphylococcus aureus* (ATCC 25923) and Gram-negative *Escherichia coli* (ATCC 25922) using the resazurin-based microtiter plate assay [45]. The bacterial strains were cultured in Mueller-Hinton broth (MHB) at 37 °C for 24 h. The bacterial suspension was adjusted to a turbidity equivalent to a 0.5 McFarland standard, corresponding to approximately 1.5×10^8 CFU/mL. The assay was performed in 96-well microplates containing the nanoemulsion formulations (PR1 - PR5 and TR1 - TR5) and bacterial suspension. A

negative control (bacteria without nanoemulsion) was included.

After incubation at 37 °C for 24 h, resazurin indicator solution (0.015%, w/v) was added to each well, and the plates were further incubated for 4 h. The antibacterial activity was assessed qualitatively based on color change: Blue indicated growth inhibition (resazurin remained unreduced), while a pink indicated bacterial growth (reduction of resazurin to resorufin). The degree of inhibition was qualitatively scored based on the extent of color change relative to the control: (+++) no inhibition (intense pink color comparable to the control), (++) weak inhibition (light pink), (+) moderate inhibition (purple or partially reduced color), and (−) complete inhibition (blue, indicating no bacterial growth).

Antioxidant and tyrosinase inhibitory activities

The antioxidant capacity and anti-melanogenic potential of the nanoemulsions were assessed using the DPPH radical scavenging assay and tyrosinase inhibition assay, respectively. The protocols followed the methods described above with minor modifications to accommodate the nanoemulsion system. For the DPPH assay, the nanoemulsion samples were mixed with the DPPH solution (0.2 mM in methanol), and the reaction was incubated in the dark at room temperature for 30 min. Absorbance was measured at 517 nm to determine the percentage of radical scavenging activity. For the tyrosinase inhibition assay, nanoemulsion samples were incubated with mushroom tyrosinase and L-DOPA substrate, and absorbance of dopachrome formation was measured at 475 nm. The percentage of inhibition for both assays was calculated relative to the control (blank emulsion without extract) to account for any background interference from the nanoemulsion components.

Statistical analysis

Results are expressed as mean ± standard deviation (SD). Data were analyzed using 1-way analysis of variance (ANOVA), followed by Duncan's multiple range test as an exploratory post hoc comparison. Statistical analyses were performed using SPSS version 26.0 (IBM Corp., Armonk, NY, USA). Differences were considered statistically significant at $p < 0.05$.

Results and discussion

Total phenolic content and antioxidant activities of rambutan peel extract

The extract exhibited a high total phenolic content (TPC) of 849.70 ± 38.20 mg GAE/g extract and strong antioxidant capacities (**Table 1**). The TPC value obtained in this study is relatively high compared to conventional crude extracts reported in the range of 45.8 - 156.8 mg GAE/g [8,9], which may be attributed to the use of ultrasound-assisted extraction that enhances mass transfer and phenolic release [10,11]. This value is also comparable to phenolic-enriched fractions reported in the literature [12], indicating the high extraction efficiency achieved in this study. The DPPH radical scavenging activity (IC_{50} = 3.53 ± 0.05 µg/mL) was in the same order of magnitude as that of ascorbic acid (3.12 ± 0.02 µg/mL) under identical assay conditions, while the ABTS assay showed moderate activity (IC_{50} = 54.63 ± 3.85 µg/mL). FRAP analysis revealed exceptional reducing power (2268.47 ± 8.50 µmol Fe^{2+}/g extract), indicating a strong electron-donating capacity to terminate oxidation chain reactions. This TPC value is consistent with previous reports of 877.11 mg GAE/g [12], confirming the efficiency of the extraction process.

Total phenolic content was expressed as gallic acid equivalents (GAE), which represent a relative index of phenolic abundance rather than the actual molar concentration of individual phenolic compounds. The observed variation between DPPH and ABTS results reflects differences in reaction mechanisms, as DPPH is sensitive to steric hindrance, whereas ABTS detects both hydrophilic and lipophilic antioxidants [26]. In addition, the marked discrepancy between DPPH and ABTS IC_{50} values can be further explained by solvent- and accessibility-related factors. The DPPH assay is typically conducted in organic solvents and primarily reflects hydrogen atom transfer (HAT) reactions, favoring antioxidants with multiple accessible hydroxyl groups and minimal steric hindrance. In contrast, the ABTS assay is performed in aqueous or mixed solvent systems and is based on both electron transfer (ET) and HAT mechanisms, enabling the detection of a broader range of antioxidant compounds.

Major constituents of the rambutan peel extract, such as geraniin and corilagin, are ellagitannins with extensive hydroxylation and considerable steric bulk,

which may differentially influence radical accessibility and apparent reaction kinetics in each assay. Consequently, lower apparent activity in the ABTS assay does not necessarily indicate weaker intrinsic antioxidant capacity, but rather reflects assay-specific physicochemical constraints. Similar discrepancies between DPPH and ABTS results have been widely reported for phenolic-rich plant extracts dominated by high-molecular-weight tannins, highlighting the method-dependent nature of antioxidant evaluation [46]. The strong antioxidant activity can be attributed to the abundance of hydroxyl-bearing phenolic compounds, such as geraniin, corilagin, and ellagic acid, which donate hydrogen atoms or electrons to neutralize free radicals [12,14,47]. Previous studies have demonstrated that rambutan peel phenolics effectively reduce intracellular reactive oxygen species (ROS) generation and enhance superoxide dismutase (SOD) activity in oxidative stress-induced cells [12]. These findings confirm that phenolic compounds are the primary contributors to the extract's antioxidant potential. It should be noted that these assays were performed as comparative screening tests rather than formal equivalence studies; therefore, the results reflect relative antioxidant potency under identical experimental conditions.

Table 1 Total phenolic content and antioxidant activities of rambutan (*Nephelium lappaceum* L.) peel extract determined by DPPH, ABTS, and FRAP assays. Values are expressed as mean ± SD (n = 3).

Samples	Total phenolic content (mg GAE/g extract)	Antioxidant activities		
		DPPH (IC_{50}; µg/mL)	ABTS (IC_{50}; µg/mL)	FRAP (µmol Fe^{2+} equivalent /g extract)
Nephelium lappaceum L.	849.70 ± 38.20	3.53 ± 0.05	54.63 ± 3.85	2,268.47 ± 8.50
Std. Ascorbic acid (AS)	-	3.12 ± 0.02	0.50 ± 0.01	-

Note: Calibration curves for antioxidant assays showed good linearity ($R^2 > 0.99$).

Anti-aging enzyme inhibitory potential

To assess anti-aging potential, the extract was evaluated for its inhibitory activity against key skin-aging enzymes, as depicted in **Figure 1**. The extract exhibited pronounced collagenase inhibitory activity with an IC_{50} of 0.089 ± 0.012 mg/mL, compared to ascorbic acid (IC_{50} = 0.066 ± 0.004 mg/mL). At matched concentrations tested in this study, the extract demonstrated substantial inhibition, indicating notable anti-collagenase activity under identical experimental conditions. For elastase inhibition, the extract showed considerably weaker activity (IC_{50} = 4.46 ± 0.63 mg/mL) than epigallocatechin gallate (EGCG) (IC_{50} = 0.015 ± 0.002 mg/mL), indicating weak elastase inhibitory potency relative to the reference compound. For tyrosinase, the extract exhibited an IC_{50} of 1.11 ± 0.020 mg/mL, whereas kojic acid showed a lower IC_{50} value of 0.311 ± 0.001 mg/mL, suggesting moderate tyrosinase inhibition.

Despite the weaker elastase inhibitory potency compared with standard inhibitors, the concurrent inhibition of collagenase and tyrosinase suggests a multi-target protective potential against skin aging. The observed bioactivities are consistent with previous reports, although variations may arise from differences in extraction conditions. For example, Lourith *et al.* [15] reported comparable collagenase and elastase inhibition for rambutan peel extract, whereas Boonpisuttinant *et al*. observed stronger tyrosinase inhibition (IC_{50} = 0.04 mg/mL) [14], likely due to differences in fruit maturity, cultivar, or extraction solvents that significantly influence phenolic composition.

Mechanistically, the enzyme inhibitory activity can be attributed to specific phenolic constituents, particularly geraniin, ellagic acid, and flavonoids. These compounds may inhibit enzymes through active-site interactions and metal ion chelation, specifically Zn^{2+} in collagenase/elastase and Cu^{2+} in tyrosinase [48]. Furthermore, since oxidative stress is known to activate matrix metalloproteinases (MMPs), the potent antioxidant activity of the extract may indirectly contribute to enzyme suppression, providing a dual-mechanism approach to mitigating skin aging.

It should be noted that the *in vitro* collagenase inhibition assay employed bacterial collagenase as a preliminary screening model, whereas molecular

docking was conducted using human MMP-1 to explore potential ligand–enzyme interactions relevant to skin aging. Owing to structural and mechanistic differences between these enzymes, the docking results are interpreted as qualitative insights into possible binding trends rather than as a direct quantitative correlation with the *in vitro* IC_{50} values.

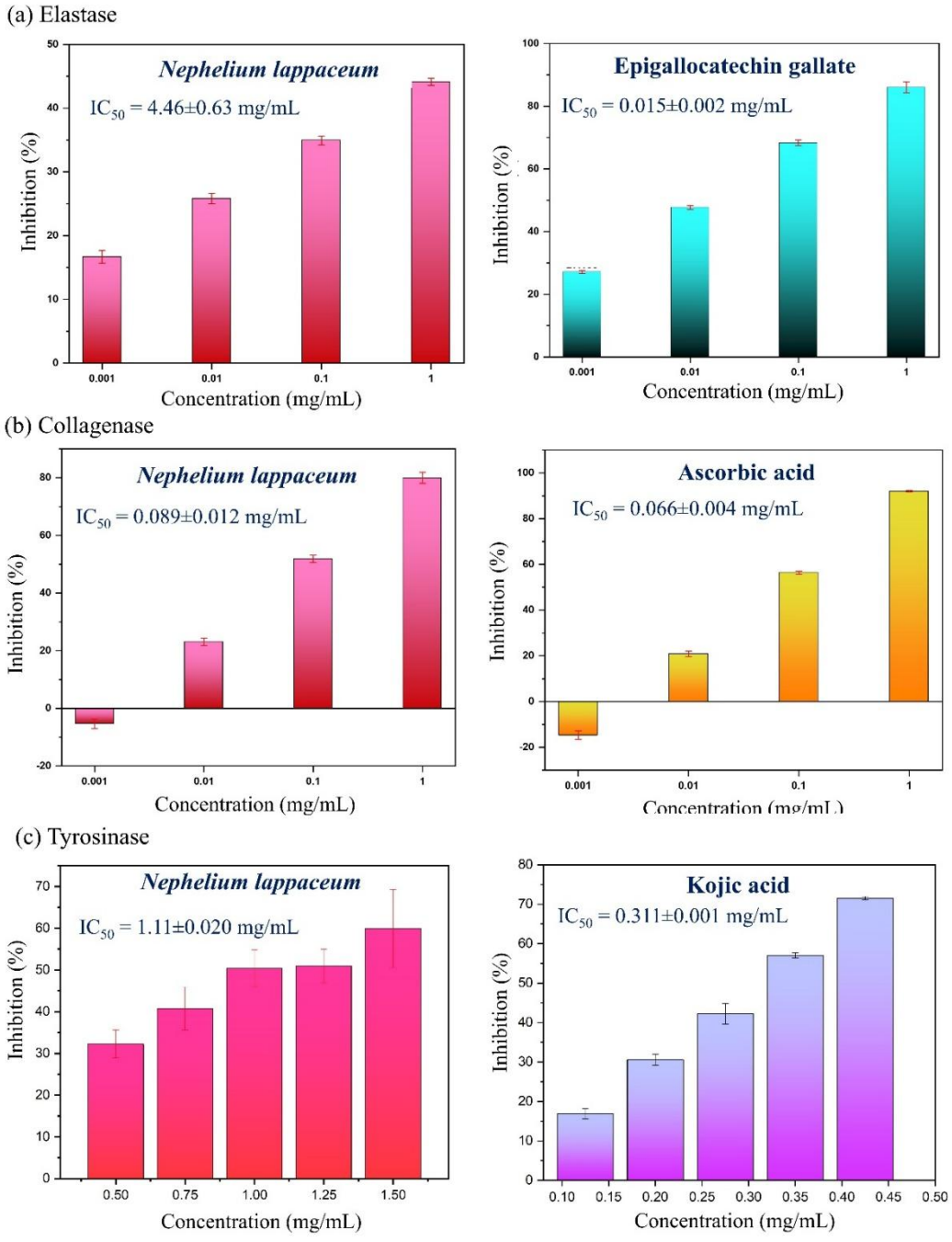

Figure 1 Enzyme inhibitory activities of rambutan peel extract compared to positive controls. (a) Elastase, (b) collagenase, and (c) tyrosinase inhibitory activities compared with epigallocatechin gallate, ascorbic acid, and kojic acid, respectively. Data are expressed as mean ± SD of 3 independent experiments. IC_{50} values indicate the concentration required for 50% enzyme inhibition. Concentration ranges were selected based on preliminary optimization to ensure reliable dose–response curves. Negative inhibition values observed at the lowest concentrations reflect experimental variability when inhibitor levels are below the effective threshold and do not indicate enzyme activation.

Identification of phytochemical compounds by LC-ESI-QTOF-MS

The LC-MS/MS chromatogram of the extract demonstrated excellent separation of bioactive metabolites across a 60-min gradient elution (**Figure 2**). The analysis identified several phytochemicals belonging to different metabolite families including phenolic acids, flavonoids, sugar acids, and ellagitannins. Based on normalized peak area percentages obtained from extracted ion chromatograms, the identified major compounds accounted for approximately 70% of the total detected LC-MS signal. No external standards or response factor corrections were applied; therefore, the reported percentages represent relative signal intensities rather than absolute mass fractions. The chemical structures of these major constituents are illustrated in **Figure 3**.

Ellagitannins constituted the major phytochemical class, with geraniin (peak 4, retention time (RT) 10.174 min) being the most abundant compound at 34.57%. Geraniin has been recognized as a characteristic bioactive marker in *Nephelium* species and exhibits potent multitarget inhibitory activities against skin aging enzymes [9]. Previous studies have demonstrated that geraniin-rich extracts effectively inhibit elastase, collagenase, and MMP-2 [14]. The inhibitory mechanism involves competitive binding to enzyme active sites via hydrogen bonding and hydrophobic interactions with aromatic residues, as well as by suppression of MMP-1, MMP-3, and MMP-9 expression in UV-induced skin photoaging models [49].

Ellagic acid (peak 5, RT 12.905 min, 16.22%) emerged as the second most abundant compound. This phenolic lactone is a powerful antioxidant and melanogenesis inhibitor, with efficacy comparable to synthetic whitening agents [50]. Its tyrosinase inhibitory mechanism involves chelating Cu^{2+} at the active site and suppressing cAMP-mediated signaling pathways [51]. A compound putatively identified as elatoside E (peak 7, RT 27.559 min, 13.62%), an oleanolic acid triterpene saponin, was tentatively assigned based on accurate mass measurement ($[M-H]^-$ m/z 881) and MS/MS fragmentation patterns in comparison with literature data. However, this identification remains preliminary in the absence of an authentic reference standard. While elatoside E is typically associated with *Aralia elata* and has not been previously reported in rambutan peel, saponin-like compounds have been documented to exhibit anti-inflammatory properties and may influence interfacial behavior in emulsified systems [52]. Minor phenolic acids detected included shikimic acid (peak 1, RT 1.654 min, 0.78%), gallic acid (peak 2, RT 4.209 min, 2.57%), and 3,4-dihydroxybenzoic acid (peak 3, RT 6.146 min, 1.56%), which contribute to the extract's broad-spectrum antioxidant capacity and ultraviolet absorption [53,54]. Additionally, quercetin (peak 6, RT 18.524 min, 0.73%) was identified as the predominant flavonoid aglycone. This flavonol is known for its broad enzyme inhibitory activity against tyrosinase, collagenase, and elastase for skin anti-aging effects [55].

Additional minor compounds were identified including α-(p-methoxyphenyl)-6-methyl-2-pyridinea crylic acid (peak 8, RT 35.352 min), linoleic acid (peak 9, RT 47.278 min), and isopalmitic acid (peak 10, RT 50.185 min), which were present at trace levels based on accurate mass matching. The predominance of geraniin and ellagic acid, which together constitute over 50% of the extract, is consistent with the strong antioxidant and enzyme inhibitory activities observed in this study. The presence of multiple hydroxyl groups and aromatic systems in these compounds enables efficient free radical scavenging and metal chelation. The rich profile of ellagitannins and their metabolites positions rambutan peel extract as a promising bioactive candidate for developing natural anti-aging cosmeceuticals.

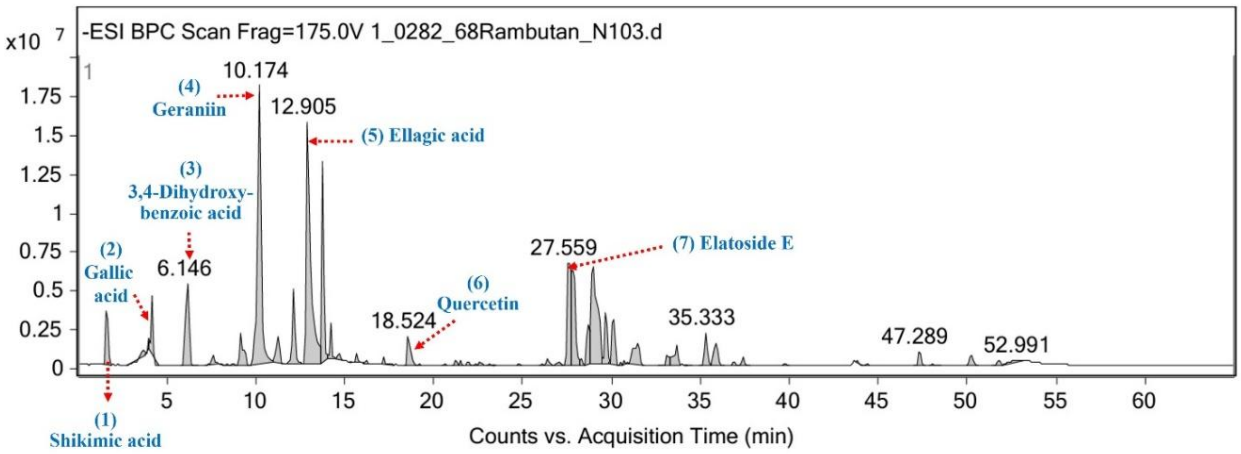

Figure 2 LC-MS/MS chromatogram of rambutan peel extract showing major phytochemical constituents detected in negative ESI mode.

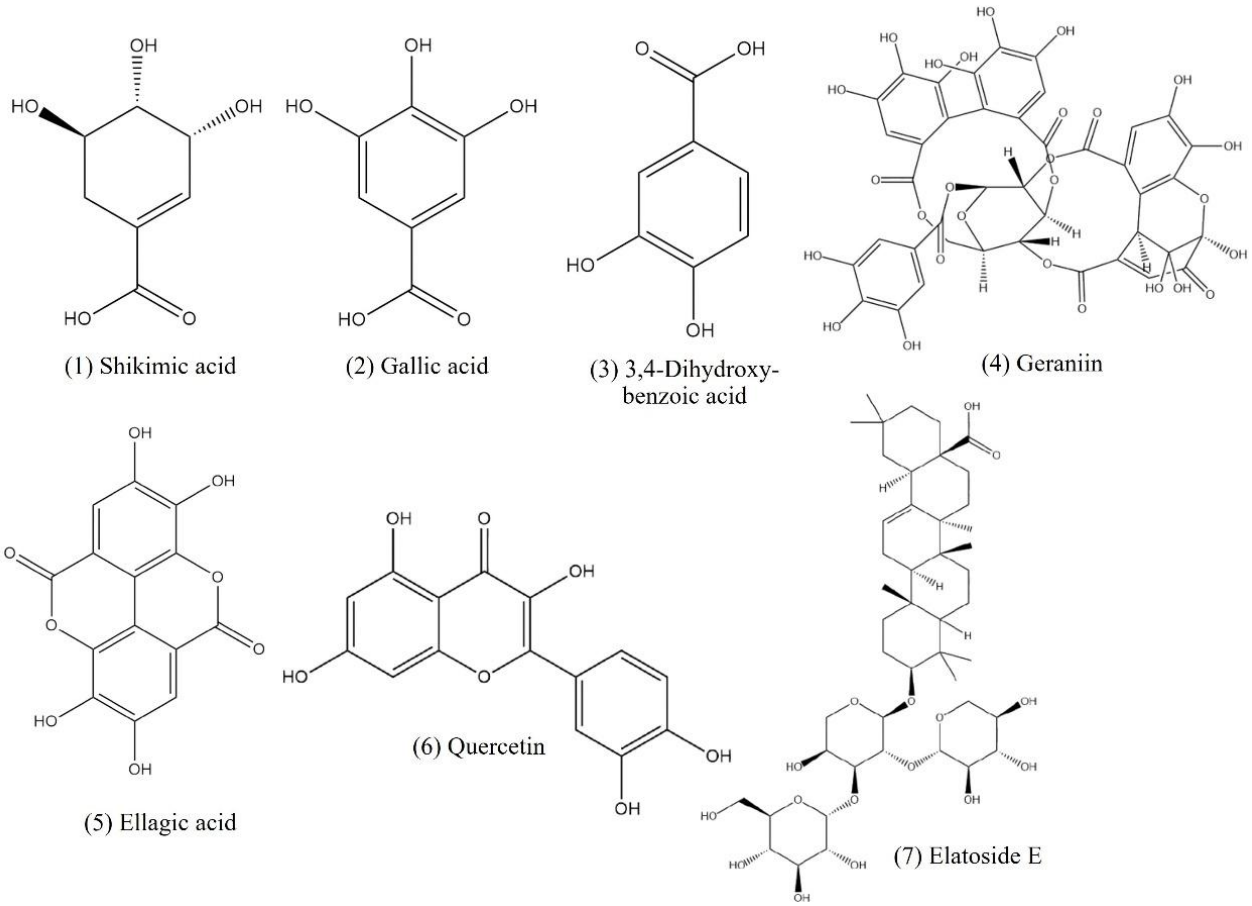

Figure 3 Chemical structures of 7 major compounds identified in rambutan peel extracts by LC-MS/MS analysis.

Molecular docking

To elucidate the molecular mechanisms underlying the observed enzyme inhibitory activities, molecular docking simulations were performed for the 7 identified phytochemicals against elastase, collagenase, and tyrosinase. The docking protocol was first validated by redocking native ligands (trifluoroacetyl-dipeptide-anilide for elastase, hydroxamate-based inhibitor for collagenase, and tropolone for tyrosinase), yielding RMSD values of 1.21 Å for elastase, 1.48 Å for collagenase, and 1.36 Å for tyrosinase (**Figures 4(A) - 4(C)**), confirming the

reliability of the docking protocol (**Table 2**). The docking grid was centered on the catalytic active site of each enzyme, defined based on the coordinates of the co-crystallized native ligands and key catalytic residues reported in the literature.

Geraniin, the most abundant compound (34.57%), exhibited among the most favorable binding energies within the tested phytochemicals for each enzyme, with docking scores of −10.32, −9.09, and −9.32 kcal/mol for elastase, collagenase, and tyrosinase, respectively. It should be noted that direct comparison of absolute binding energies across different enzymes is not appropriate, and the large molecular size of geraniin may contribute to lower docking energies due to increased van der Waals interactions. These favorable energies were supported by high cluster percentages (53% - 82%), indicating thermodynamically stable binding conformations.

Docking scores are reported as predicted binding free energies and are influenced by ligand size and contact surface. Therefore, absolute binding energies should not be directly compared across ligands with substantially different molecular weights, nor interpreted as quantitative predictors of inhibitory potency. In this study, docking results were interpreted primarily based on binding modes and key residue interactions rather than score ranking alone. Molecular interaction analysis (**Table 3)** revealed that geraniin established an extensive hydrogen bonding network with critical active site residues. In elastase, geraniin formed hydrogen bonds with Cys45, His60, Asp100, Asp101, Val103, Gln200, Ser203, Ser222, and Val224, effectively blocking substrate access (**Figure 4(D)**). For collagenase, key interactions involved Ser602, Trp604, Met605, and Asn608 (**Figure 4(E)**), while in tyrosinase, the compound interacted with Asn81, His224, Asn260, and Gly281 (**Figure 4(F)**). These multiple interactions explain geraniin's multitarget inhibitory potential and are consistent with previous findings showing that geraniin-rich extracts inhibit elastase by 31.08% and collagenase by 53.99% [15], as well as its high affinity for diverse protein targets [56]. Ligand efficiency normalization was not applied in this study and should be considered in future work for size-independent comparison of binding performance.

Ellagic acid (16.22%) demonstrated moderate-to-strong binding affinities, particularly against tyrosinase (-6.64 kcal/mol) and elastase (−5.79 kcal/mol), facilitated by its planar aromatic structure (**Figures 4(G) - 4(I)**). It formed stable interactions with Thr182, Val224, and Arg226 in elastase **(Table 3)**. In the tyrosinase active site, it established a robust network including Asn260, Met280, Gly281, Ser282, and His296, potentially disrupting the copper-coordinating center essential for catalysis. Although the binding energy for collagenase was moderate (−3.18 kcal/mol), interaction with Asn608 was observed, contributing to overall inhibition alongside geraniin. It should be noted that all crystallographic water molecules were removed prior to docking, which may limit the ability of the model to capture water-mediated interactions, particularly for polyphenolic ligands with multiple hydroxyl groups. Therefore, the docking results should be interpreted as qualitative insights into binding modes rather than definitive quantitative predictions.

Among minor compounds and controls, 3,4-dihydroxybenzoic acid exhibited a high cluster population (81%) for elastase (−4.43 kcal/mol), suggesting highly specific binding despite its smaller molecular size. The positive controls, EGCG and kojic acid, displayed strong affinities for elastase and tyrosinase, respectively. However, ascorbic acid, the collagenase positive control, exhibited relatively weak binding (−3.84 kcal/mol) despite its potent experimental efficacy, highlighting a known limitation of classical docking approaches, which are less suited to model metal-chelation- or redox-driven inhibitory mechanisms. Therefore, docking results were used to infer plausible binding modes rather than to predict inhibitory potency [57].

The molecular docking results provide structural support for the experimentally observed enzyme inhibition by highlighting plausible ligand–enzyme interaction patterns and key active-site residues. The superior collagenase inhibition observed experimentally (IC_{50} = 0.089 mg/mL) is consistent with geraniin's extensive interactions with Trp604 and Asn608. For tyrosinase, the combined targeting of His224 by geraniin and His296 by ellagic acid likely enhances active-site blockade. In this study, molecular docking was employed as a qualitative tool to explore ligand–enzyme interaction patterns rather than as a quantitative predictor of inhibitory activity.

Table 2 *In silico* docking scores and cluster analysis of major compounds from rambutan peel extract against elastase, collagenase, and tyrosinase.

Ligand molecule	Elastase		Collagenase		Tyrosinase	
	Score (kcal/mol)	% Cluster	Score (kcal/mol)	% Cluster	Score (kcal/mol)	% Cluster
(1) Shikimic acid	−3.97	47	−3.27	54	−3.27	42
(2) Gallic acid	−4.31	63	−3.29	40	−3.20	30
(3) 3,4 −Dihydroxybenzoic acid	−4.43	81	−3.60	28	−3.39	46
(4) Geraniin	−10.32	53	−9.09	58	−9.32	82
(5) Ellagic acid	−5.79	74	−3.18	62	−6.64	82
(6) Quercetin	−6.64	24	−2.36	31	−5.49	60
(7) Elatoside E	−4.59	6	−5.07	41	−1.42	4
[a] Ascorbic acid	−3.71	15	−3.84	14	−3.35	21
[b] Epigallocatechin gallate (EGCG)	−8.53	20	−4.40	28	−5.73	9
[c] Kojic acid	−3.36	70	−4.26	68	−4.17	78

Note: Binding energies may be influenced by ligand size; therefore, compounds with higher molecular weights (e.g., geraniin) may exhibit more favorable docking scores due to increased van der Waals interactions. Direct comparison of absolute binding energies between ligands of different sizes should be interpreted with caution. Binding scores are reported as predicted binding free energy (Score, kcal/mol) obtained from AutoDock 4.2. The cluster percentage (% Cluster) represents the proportion of docking conformations within the most populated cluster based on root-mean-square deviation (RMSD) analysis. Molecular docking simulations were performed using the Lamarckian Genetic Algorithm (LGA). [a] Ascorbic acid was used as a positive control for the collagenase inhibition assay. [b] Epigallocatechin gallate (EGCG) was used as a positive control for the elastase inhibition assay. [c] Kojic acid was used as a positive control for the tyrosinase inhibition assay.

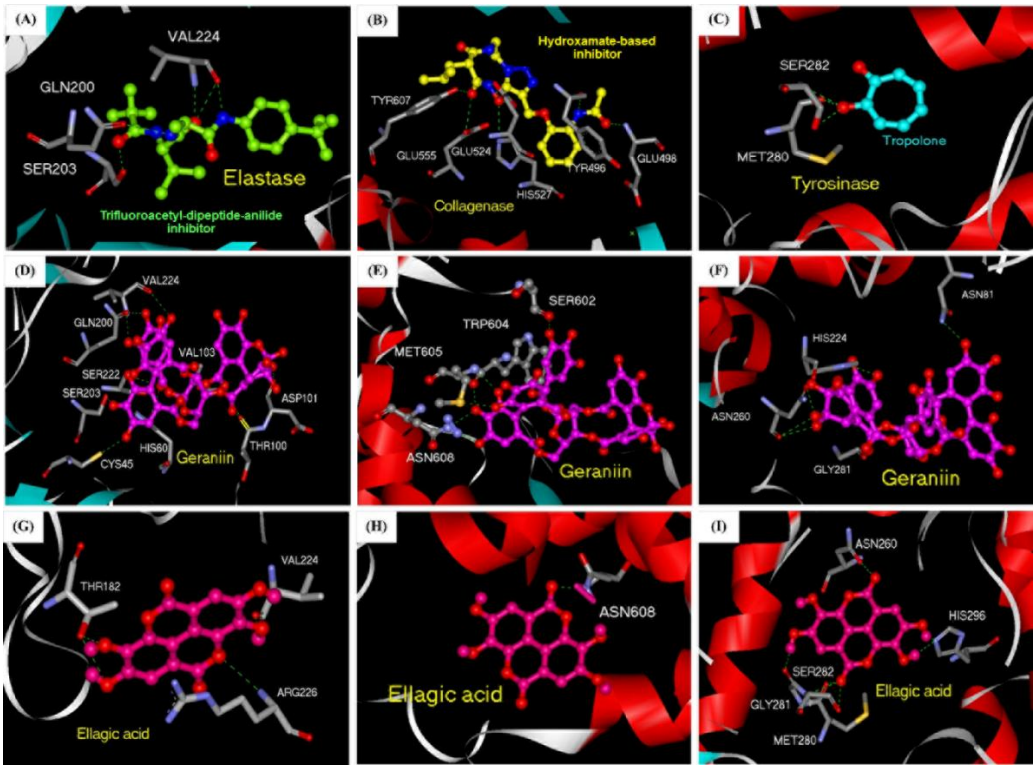

Figure 4 Molecular docking interactions of rambutan peel extract compounds with skin-aging enzymes. (A-C) Validation of the docking protocol using co-crystallized inhibitors in elastase, collagenase, and tyrosinase, respectively. (D-F) Binding modes of geraniin with elastase, collagenase, and tyrosinase. (G-I) Binding interactions of ellagic acid with elastase, collagenase, and tyrosinase. Key interacting amino acid residues involved in hydrogen bonding and catalytic interactions are labeled. Hydrogen bonds are indicated by dashed lines.

Table 3 Hydrogen bonding interactions of geraniin and ellagic acid with elastase, collagenase, and tyrosinase active site residues.

Ligand	Active site residues involved in hydrogen bonding		
	Elastase	**Collagenase**	**Tyrosinase**
Geraniin	O43 ----- His60	O47 ----- Met605	O45 ----- Gly281
	O43 ----- Ser222	O51 ----- Met605	O49 ----- Asn81
	O44 ----- Val103	O52 ----- Trp604	O54 ----- His224
	O44 ----- Asp100	O52 ----- Asn608	O58 ----- Asn260
	O45 ----- Asp100	O53 ----- Asn608	O59 ----- Asn260
	O52 ----- Ser203	O68 ----- Ser602	
	O53 ----- Cys45		
	O58 ----- Asp101		
	O66 ----- Val224		
	O67 ----- Gln200		
	O68 ----- Gln200		
Ellagic acid	O1 ----- Arg226	O7 ----- Asn608	O3 ----- His296
	O3 ----- Val224		O5 ----- His296
	O4 ----- Thr182		O6 ----- Gly281
	O6 ----- Thr182		O7 ----- Ser282
			O7 ----- Met280
			O8 ----- Asn260

Nanoemulsion formulation and characterization

Nanoemulsions provide several critical advantages for cosmeceutical applications including enhanced solubilization of hydrophobic actives within oil droplets, protection of labile compounds from oxidative degradation, controlled and sustained release, and increased bioavailability [58]. To prepare extract-loaded nanoemulsions for cosmetic applications, oil-in-water emulsions were developed using olive oil as the oil phase with 2 surfactant systems: Polyethylene glycol 400 (PEG400) and polysorbate 80 (Tween 80). Ten formulations with varying oil:surfactant:water ratios (1:X:Y, where X = 1 - 20) were prepared and evaluated for physical stability, morphological characteristics, and physicochemical properties over a 7-day storage period (**Table 4**). These formulations were generated using a systematic ratio-screening approach rather than a formal design-of-experiments model, with surfactant concentrations selected based on preliminary trials and literature reports to identify stable formulation windows suitable for cosmetic applications.

All formulations exhibited excellent short-term stability without phase separation, creaming, or sedimentation, confirming successful emulsion formation. Visual inspection revealed transparent appearance for PEG400-based emulsions (PR1–PR5) and low-concentration Tween 80 formulations (TR1–TR2), while higher Tween 80 concentrations (TR3–TR5) produced clear solutions. Viscosity measurements demonstrated distinct surfactant-dependent patterns: PEG400 formulations showed moderate viscosity increases (1.19 ± 0.06 to 6.22 ± 0.05 mPa·s), whereas Tween 80 systems exhibited significantly higher viscosity at elevated concentrations, reaching 30.9 ± 0.04 mPa·s for TR5, reflecting Tween 80's superior viscosity-modifying capacity.

Microscopic analysis revealed concentration-dependent morphological differences (**Figure 5**). PEG400 emulsions showed increasing droplet size with higher surfactant concentrations, with PR1 (1:1:48) displaying small, uniform droplets while PR5 (1:20:29) exhibited larger aggregated droplets due to micelle formation. This behavior reflects the dual role of PEG400 as both surfactant and co-surfactant/co-solvent, where excessive concentrations may promote micellar solubilization rather than interfacial stabilization [59]. Conversely, Tween 80 formulations demonstrated inverse behavior, with TR1 (1:1:48) showing numerous small droplets and TR5 (1:20:29) displaying fewer droplets attributed to increased viscosity inhibiting droplet formation. Based on droplet size uniformity and

optimal dispersion characteristics, PR1 and PR2 were selected for physicochemical characterization using dynamic light scattering (DLS).

Dynamic light scattering analysis revealed that the extract plays a crucial stabilizing role (**Table 5**). Extract-loaded formulations (PR1: 266.7 ± 6.34 nm; PR2: 275.5 ± 5.16 nm) exhibited 3 - 5-fold smaller particle sizes compared to blank controls (B1: 872.8 ± 20.72 nm; B2: 1,388.0 ± 30.42 nm). Although classical nanoemulsions are often defined as having droplet sizes below 200 nm [60], the formulations obtained in this study (266 - 275 nm) remain within the nanometric scale and are therefore suitable for preliminary cosmetic formulation screening rather than final commercial products.

This dramatic size reduction can be attributed to the amphiphilic nature of phenolic compounds, particularly geraniin and ellagic acid, which possess both hydrophobic aromatic rings and hydrophilic hydroxyl groups. These structural features may facilitate the adsorption of phenolic compounds at the oil-water interface, potentially contributing to reduced interfacial tension and enhanced emulsion stability, as suggested in previous studies [61]. However, direct interfacial tension measurements were not performed in this study. Similar enhancement of nanoemulsion stability by fruit peel bioactive compounds has been reported for *Cordia myxa* peel extract, where phenolic-rich extracts improved both antioxidant activity and antimicrobial properties of the encapsulated system compared to free formulations [62].

Polydispersity index (PDI) values indicated moderately polydisperse particle size distributions for extract-loaded emulsions (PR1: 0.332 ± 0.024; PR2: 0.325 ± 0.017), which are considered acceptable for preliminary cosmetic nanoemulsion screening, although further optimization would be required to achieve narrower distributions (PDI < 0.2) for pharmaceutical-grade applications. In contrast, blank B2 showed severe destabilization (PDI = 0.724 ± 0.076). Zeta potential measurements confirmed excellent colloidal stability (PR1: +32.7 ± 0.404 mV; PR2: + 32.6 ± 0.216 mV), with values exceeding the + 30-mV threshold, indicating strong electrostatic repulsion preventing aggregation. Conductivity analysis demonstrated extract-dependent behavior, with PR1 (0.0753 ± 0.00045 mS/cm) and PR2 (0.1020 ± 0.00100 mS/cm) showing higher conductivity than blank formulations (B1: 0.0278 ± 0.00507 mS/cm), indicating that phenolic compounds likely contribute ionic species that enhance system stability. These results demonstrate that rambutan peel extract functions as a multifunctional additive providing interfacial modification, electrosteric stabilization arising from charged phenolic groups and steric hindrance at the oil-water interface, and appropriate viscosity modulation. PR1 emerged as the optimal formulation with nanometric particle size (266.7 nm), moderate PDI (0.332), high zeta potential (+32.7 mV), and suitable conductivity for cosmetic applications.

Table 4 Physical characteristics of extract-loaded nanoemulsions.

Formulation code	Surfactant system (Oil: PEG400/Tween 80: water)	Visual inspection	Viscosity (mPa·s)	Phase separation	Droplet size observation
PR1	1:1:48	Transparent	1.19 ± 0.06	No	Small, uniform
PR2	1:2:47	Transparent	ND	No	Small to medium
PR3	1:5:44	Transparent	ND	No	Medium
PR4	1:10:39	Transparent	2.57 ± 0.05	No	Medium to large
PR5	1:20:29	Transparent	6.22 ± 0.05	No	Large, aggregated
TR1	1:1:48	Transparent	1.15 ± 0.04	No	Small, numerous
TR2	1:2:47	Transparent	ND	No	Small, moderate density
TR3	1:5:44	Clear	ND	No	Reduced density
TR4	1:10:39	Clear	ND	No	Fewer droplets
TR5	1:20:29	Clear	30.9 ± 0.04	No	Significantly fewer droplets

ND = Not Determined. Droplet characteristics were assessed by optical microscopy at 40× magnification. Transparent indicates minimal light scattering, while clear refers to slightly turbid but homogeneous systems.

It should be noted that the stability evaluation in this study was limited to a short-term storage period of 7 days, which is sufficient for preliminary screening and formulation selection. Additional stress stability tests (e.g., centrifugation, thermal cycling, and pH variation) were not conducted and should be addressed in future work to further substantiate long-term and commercial-scale formulation robustness. Therefore, extended stability studies under accelerated and real-time storage conditions are warranted to confirm the shelf-life of the optimized nanoemulsion.

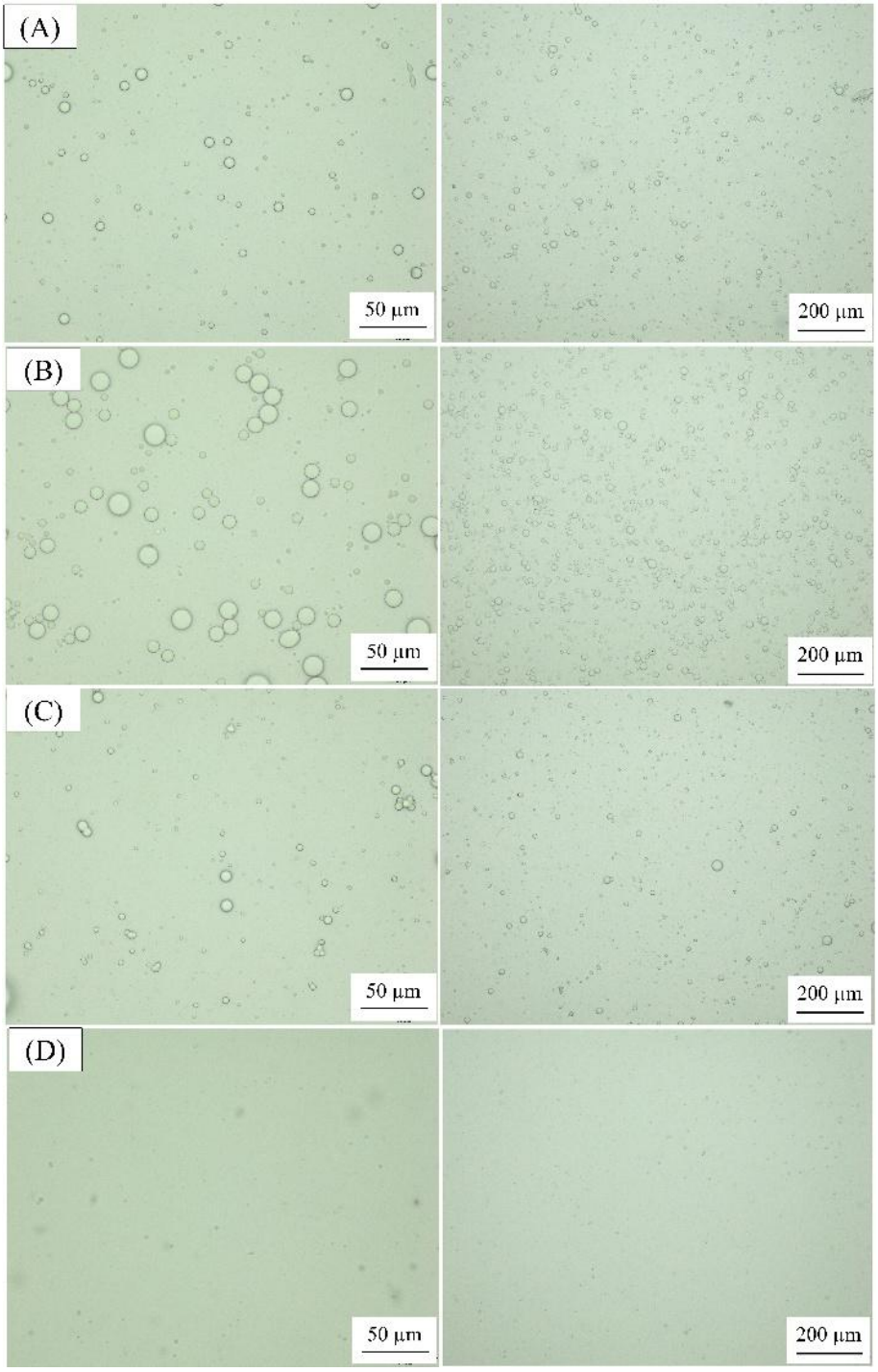

Figure 5 Bright-field optical microscopy images of extract-loaded nanoemulsions; (a) PR1, (b) PR5, (c) TR1, and (d) TR5 formulations at 50 µm (left) and 200 µm (right) magnifications.

Table 5 Physicochemical properties of extract-loaded and blank nanoemulsion formulations.

Formulations	Z-average size diameter (nm)	Polydispersity index (PDI)	Zeta potential (mV)	Conductivity (mS/cm)
PR1	266.7 ± 6.34[a]	0.332 ± 0.024[a]	32.7 ± 0.404[a]	0.0753 ± 0.00045[b]
PR2	275.5 ± 5.16[a]	0.325 ± 0.017[a]	32.6 ± 0.216[a]	0.1020 ± 0.00100 [a]
B1	872.8 ± 20.72[b]	0.291 ± 0.027[a]	32.9 ± 1.310[a]	0.0278 ± 0.00507[c]
B2	1,388.0 ± 30.42[c]	0.724 ± 0.076[b]	28.4 ± 1.02[b]	0.0310 ± 0.00072[c]

Note: Z-average size diameter, polydispersity index (PDI), zeta potential, and conductivity were measured to evaluate particle size distribution and colloidal stability. PR1 and PR2 represent extract-loaded nanoemulsions, while B1 and B2 denote blank formulations without rambutan peel extract. Values are expressed as mean ± standard deviation (SD) (n = 3). Different superscript letters within the same column indicate statistically significant differences at $p < 0.05$, as determined by 1-way analysis of variance (ANOVA) followed by Duncan's multiple range test.

Biological activity evaluation of extract-loaded nanoemulsions

Antibacterial activity

Nanoemulsion formulations were evaluated against Gram-positive *Staphylococcus aureus* (ATCC 25923) and Gram-negative *Escherichia coli* (ATCC 25922) using a resazurin-based metabolic indicator assay (**Figure 6** and **Table 6**) as a qualitative screening tool. Against *S. aureus*, formulations PR1–PR3 and TR1–TR4 exhibited no detectable metabolic activity under the tested conditions, as indicated by purple color retention, whereas formulations containing higher surfactant concentrations (PR4–PR5 and TR5) allowed bacterial growth, suggesting reduced antibacterial performance. This inverse trend, observed in this qualitative assay, suggests that excessive surfactant may sequester phenolic compounds within micellar structures, thereby limiting their bioavailability.

For *E. coli*, a Gram-negative bacterium characterized by a lipopolysaccharide-rich outer membrane conferring intrinsic resistance, only PR1–PR2 achieved complete inhibition in this qualitative assay, indicating comparatively enhanced broad-spectrum performance among the tested formulations. The formulation-dependent response against *E. coli* likely reflects surfactant-specific interactions with bacterial membrane architecture. Notably, Tween 80 at high concentration (TR5) also showed growth inhibition, which may be attributed to membrane-permeabilizing effects of the surfactant acting synergistically with phenolic constituents. The observed antibacterial effects are consistent with previous reports describing ellagitannins, particularly geraniin, as agents capable of disrupting bacterial membrane integrity and interfering with key metabolic enzymes [63]. The differential susceptibility between Gram-positive and Gram-negative bacteria can be explained by structural differences in their cell envelopes, with the peptidoglycan-rich wall of *S. aureus* being more permeable to phenolic compounds than the outer membrane barrier of *E. coli*.

Antioxidant and anti-tyrosinase activities

To assess bioactivity retention following nanoemulsion formulation, antioxidant and anti-tyrosinase activities were evaluated (**Table 6**). Both surfactant systems retained high DPPH radical scavenging activity (91.07% - 95.63%) across all formulations, indicating effective preservation of antioxidant function after encapsulation. This level of retention is comparable to that of the crude extract (IC_{50} = 3.53 μg/mL, similar to ascorbic acid) and suggests that nanoemulsion encapsulation protects phenolic compounds from oxidative degradation while maintaining their radical-quenching capacity [55]. Based on their favorable physicochemical characteristics and qualitative antibacterial performance, PR1 and PR2 were further evaluated for tyrosinase inhibition. Both formulations exhibited appreciable inhibitory activity (PR1: 44.28 ± 7.78%; PR2: 43.36 ± 10.50%), indicating that encapsulation does not hinder phenolic accessibility to enzyme active sites, potentially facilitated by the nanometric particle size (266.7 - 275.5 nm). Therefore, comparisons among

formulations in this study should be interpreted as relative differences in metabolic response rather than absolute antibacterial potency.

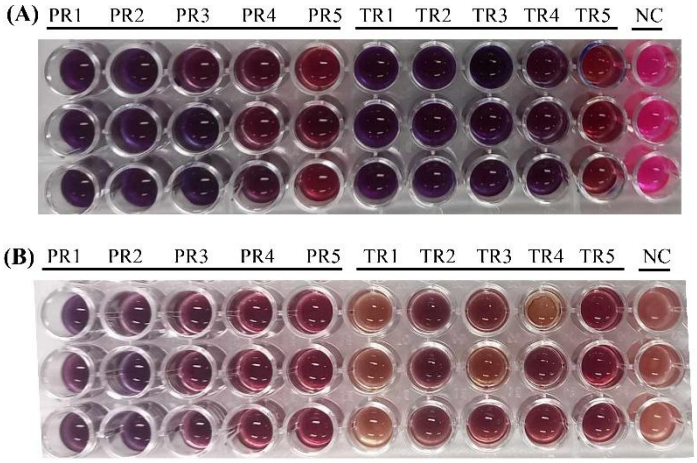

Figure 6 Antibacterial activity of extract-loaded nanoemulsions against (A) *Staphylococcus aureus* ATCC 25923 and (B) *Escherichia coli* ATCC 25922 assessed by resazurin assay. Blue/purple color indicates bacterial growth inhibition; pink to red color indicates bacterial growth. NC, negative control (bacteria without nanoemulsion). Each formulation was tested in triplicate.

Table 6 Biological activities of extract-loaded nanoemulsions. Values are expressed as mean ± SD (n = 3).

Formulation	*S. aureus* ATCC 25923	*E. coli* ATCC 25922	% DPPH inhibition	% Tyrosinase inhibition
PR1	-	-	95.63 ± 0.97[a]	44.28 ± 7.78[a]
PR2	-	-	93.60 ± 2.07[a]	43.36 ± 10.50[a]
PR3	-	+	92.69 ± 3.89[a]	ND
PR4	+	+	93.90 ± 2.99[a]	ND
PR5	+	+	92.11 ± 5.92[a]	ND
TR1	-	++	94.20 ± 2.74[a]	ND
TR2	-	+	91.82 ± 1.88[a]	ND
TR3	-	+	94.14 ± 2.22[a]	ND
TR4	-	+	91.07 ± 1.65[a]	ND
TR5	+	+	95.49 ± 6.82[a]	ND
Negative control (NC)	+++	+++	ND	ND
Blank	ND	ND	5.2 ± 1.3[b]	2.1 ± 0.8[b]

Note: Antibacterial activity determined by resazurin assay against *S. aureus* ATCC 25923 and *E. coli* ATCC 25922: (−) complete inhibition; (+) partial inhibition; (++) moderate inhibition; (+++) no inhibition. Values are mean ± SD (n = 3). Different superscript letters within the same column indicate significant differences ($p < 0.05$) by Duncan's multiple range test. ND = not determined. NC = (growth medium without nanoemulsion). Blank = nanoemulsion without extract. The qualitative scoring system was used solely for rapid formulation-level screening and is not intended to represent antibacterial potency or substitute for MIC/MBC determination.

Overall, the preservation of multifunctional bioactivities, antibacterial, antioxidant, and anti-tyrosinase, together with suitable physicochemical properties (PDI 0.325 - 0.332; zeta potential +32.6 to

+32.7 mV), supports the potential of these nanoemulsions as delivery systems for anti-aging cosmeceutical applications. It should be noted that antibacterial activity in this study was assessed using a qualitative resazurin assay for comparative screening purposes. Quantitative determination of minimum inhibitory concentration (MIC) and minimum bactericidal concentration (MBC), for example by spectrophotometric resazurin reduction or broth microdilution assays, will be required for definitive potency evaluation in future studies.

Mechanistic interpretation, structure-activity relationships, and formulation-enabled bioavailability

Taken together, the inhibitory activities observed in this study are comparable to or stronger than those previously reported for fruit peel extracts rich in ellagitannins. Notably, rambutan peel extract exhibited collagenase inhibition with an IC_{50} of 0.089 mg/mL, which is stronger than values reported for pomegranate peel extract ($IC_{50} \approx 0.15$ - 0.30 mg/mL) and mangosteen pericarp extract ($IC_{50} \approx 0.12$ mg/mL) [12,15]. In contrast, elastase inhibition fell within the range commonly reported for polyphenol-rich botanical extracts but remained weaker than purified EGCG, highlighting the influence of compound complexity and matrix effects in crude plant extracts [14,47].

The stronger inhibition observed against collagenase compared with elastase can be attributed to fundamental differences in enzyme architecture and inhibition mechanisms. Collagenase is a Zn^{2+}-dependent metalloproteinase and is therefore particularly susceptible to inhibition by polyphenolic compounds capable of metal chelation and extensive hydrogen bonding. Ellagitannins such as geraniin possess multiple hydroxyl and carbonyl groups that may interact with residues surrounding the catalytic Zn^{2+} site, resulting in effective enzyme suppression. In contrast, elastase is a serine protease with a narrower active-site pocket, which may restrict access of large polyphenolic molecules, leading to comparatively weaker inhibition despite favorable docking interactions [15,56].

Structure–activity relationship analysis based on molecular docking further supports these observations. Molecular size, hydroxyl group density, and conformational flexibility emerged as critical determinants of inhibitory behavior. Geraniin, a high-molecular-weight ellagitannin, exhibited extensive hydrogen-bonding networks with catalytic and substrate-recognition residues, supporting its multitarget inhibitory potential. However, its large molecular size may limit diffusion and accessibility within certain enzyme active sites, explaining discrepancies between docking scores and experimental potency. Conversely, smaller phenolics such as ellagic acid displayed moderate binding energies but favorable planar aromatic structures that facilitated stable interactions within narrower active sites, particularly for tyrosinase. These findings suggest that binding modes and residue engagement are more informative than absolute docking energies alone when interpreting polyphenol-enzyme interactions [56,57].

Beyond molecular interactions, the enhanced stability of extract-loaded nanoemulsions can be explained by a combination of electrostatic and steric stabilization mechanisms. Phenolic constituents likely contribute surface charges, as reflected by increased zeta potential values (+32.6 to +32.7 mV), promoting electrostatic repulsion between droplets. In addition, adsorption of polyphenols at the oil-water interface may introduce steric hindrance, further preventing coalescence. The reduced droplet size observed in extract-loaded formulations compared with blank systems supports interfacial modification by phenolic compounds, although direct interfacial tension measurements were not performed and warrant future investigation [61,62].

Nanoemulsions with droplet sizes in the range of 200–300 nm has been reported to be favorable for dermal delivery by facilitating diffusion through the stratum corneum and follicular pathways [58,61]. Accordingly, the optimized formulation (PR1), with a mean particle size of 266.7 nm and moderate polydispersity, is expected to potentially improve topical bioavailability of phenolic compounds compared with crude extracts. Moreover, encapsulation within nanoemulsion droplets may protect labile polyphenols from oxidative degradation on the skin surface, enabling sustained release and prolonged biological activity. Although *in vivo* skin permeation studies were beyond the scope of this work, the physicochemical characteristics obtained support the potential of this

nanoemulsion system as a promising delivery platform for topical cosmeceutical applications.

Study limitations and future perspectives

Despite the promising bioactivities and formulation performance demonstrated in this study, several limitations should be acknowledged to ensure appropriate interpretation of the results and to guide future research toward translational cosmeceutical development.

First, enzyme inhibition assays were conducted using bacterial collagenase rather than human matrix metalloproteinase-1 (MMP-1). Although bacterial collagenase is widely employed as a preliminary screening model for collagenolytic activity, structural and mechanistic differences between bacterial enzymes and human MMPs limit direct extrapolation to clinical relevance. Accordingly, future studies should incorporate human-relevant enzyme models to better assess anti-aging efficacy. Second, variations in rambutan cultivar, geographic origin, and fruit maturity were not strictly controlled. Such factors are known to influence polyphenolic composition and may affect reproducibility and batch-to-batch consistency. Standardization of raw material sourcing and phytochemical profiling will therefore be essential for future scale-up and commercial application. Third, phytochemical identification was primarily based on LC–MS database matching, and authentic standards were not available for all detected compounds. While this approach is acceptable for exploratory profiling, quantitative confirmation using reference standards and absolute quantification would strengthen chemical characterization and structure–activity relationship analysis.

Regarding formulation performance, nanoemulsion stability was evaluated only over a short-term storage period of 7 days. Although sufficient for preliminary screening and formulation selection, this timeframe does not reflect long-term storage requirements for cosmetic products. Extended stability studies under accelerated and real-time conditions, as well as stress tests such as centrifugation, thermal cycling, and pH variation, are necessary to establish shelf-life and commercial robustness. Biological evaluations were limited to *in vitro* enzyme assays and qualitative antibacterial screening using a resazurin-based metabolic indicator. While useful for comparative screening, these assays do not directly predict *in vivo* efficacy or clinical performance. Quantitative antibacterial evaluation (e.g., MIC and MBC determination), dose–response optimization, and mechanistic cellular studies are required for more definitive biological assessment. Furthermore, nanoemulsions were tested at a single extract concentration, and systematic dose optimization was not performed. Future studies should explore concentration-dependent effects to define optimal loading levels that balance bioactivity, stability, and safety.

From a cosmeceutical development perspective, safety and regulatory considerations were beyond the scope of the present work. Comprehensive toxicological assessments, including cytotoxicity, skin irritation, and sensitization studies, will be required in accordance with cosmetic regulatory frameworks. In addition, feasibility of scale-up, cost-effectiveness compared with conventional antioxidants, and compliance with regulatory guidelines should be evaluated to support potential industrial translation.

Overall, while the present study provides strong preliminary evidence supporting the multifunctional bioactivity and formulation potential of rambutan peel extract-loaded nanoemulsions, these limitations define the scope of interpretation and highlight critical directions for future research aimed at advancing toward practical cosmeceutical applications.

Conclusions

This study provides *in vitro* evidence supporting the bioactive potential of rambutan peel extract and its feasibility for incorporation into nanoemulsion delivery systems. The extract exhibited strong antioxidant and enzyme inhibitory activities, which were associated with its high phenolic content, particularly geraniin and ellagic acid. Molecular docking analyses further supported the multitarget interaction of major phenolics with skin-aging-related enzymes. The successful formulation of stable extract-loaded nanoemulsions with nanoscale particle sizes demonstrated that phenolic constituents can contribute to formulation stability without compromising bioactivity. Importantly, antioxidant, antibacterial, and anti-tyrosinase activities were retained following encapsulation, indicating preservation of functional properties at the formulation

level. While the biological activities reported here were evaluated using *in vitro* and qualitative screening assays, the findings establish a proof-of-concept for the valorization of rambutan peel as a functional raw material and highlight its potential relevance to cosmetic formulation research. Further studies involving quantitative antimicrobial assays, skin-relevant models, and formulation performance testing will be required to substantiate efficacy in practical cosmetic applications.

Acknowledgements

The authors acknowledge financial support from the National Higher Education, Science, Research and Innovation Policy Council through Thaksin University's Fundamental Research Fund (Grant No. FF2568-203342) for Fiscal Year 2025. We extend our appreciation to the Department of Chemistry, Faculty of Science and Digital Innovation, Thaksin University, Thailand for providing access to research facilities, computational resources, and software packages. Technical assistance provided by the Innovative Material Chemistry for Environment Center, Thaksin University, Thailand is gratefully acknowledged.

Declaration of generative AI in scientific writing

The authors used Claude (Anthropic), an artificial intelligence language model, to improve language clarity and writing quality. This AI assistance was applied under direct human supervision and control. The AI tool was used only for linguistic improvements and did not participate in experimental design, data collection, data analysis, interpretation, or scientific conclusions. All responsibility for the research content, interpretations, and findings rests with the authors.

CRediT author statement

Panita Kongsune: Conceptualization; Methodology; Formal analysis; Supervision; Writing - review & editing. **Parichat Thepthong**: Methodology; Validation; Formal analysis; Supervision; Writing - review & editing. **Khwanchanok Matpoom**: Investigation; Formal analysis; Data curation; Visualization; Writing - original draft. **Wilasinee Langmuang**: Investigation; Data curation; Validation; Writing - review & editing. **Luksika Kongjun**: Investigation; Data curation. **Netnapa Chana**: Conceptualization; Methodology; Resources; Supervision; Project administration; Funding acquisition; Writing - review & editing.

References

[1] Z Wang, F Yuan, X Zhong, S Feng and T Song. Skin microbiome and skin aging: Emerging strategies for manipulation. *Microbiological Research* 2025; **300**, 128285.

[2] NH Hussen, SK Abdulla, NM Ali, VA Ahmed, AH Hasan and EE Qadir. Role of antioxidants in skin aging and the molecular mechanism of ROS: A comprehensive review. *Aspects of Molecular Medicine* 2025; **5**, 100063.

[3] RI Amer, SM Ezzat, NM Aborehab, MF Ragab, D Mohamed, A Hashad, D Attia, MM Salama and MH El Bishbishy. Downregulation of MMP1 expression mediates the anti-aging activity of *Citrus sinensis* peel extract nanoformulation in UV induced photoaging in mice. *Biomedicine & Pharmacotherapy* 2021; **138**, 111537.

[4] A Bhardwaj, B Saroha, P Bishnoi, G Kumar, R Kumar and S Kumar. Kojic acid - a blossoming scaffold of biological significance: An overview of synthesis, properties, and biological applications. *Current Organic Chemistry* 2025; **29(17)**, 1321-1332.

[5] M Xie, Z Jiang, X Lin and X Wei. Application of plant extracts cosmetics in the field of anti-aging. *Journal of Dermatology Science and Cosmetic Technology* 2024; **1(2)**, 100014.

[6] Đ Ivković, F Andrić, M Senćanski, T Stević, M Krstić Ristivojević and P Ristivojević. Innovative analytical methodology for skin anti-aging compounds discovery from plant extracts: Integration of high-performance thin-layer chromatography-*in vitro* spectrophotometry bioassays with multivariate modeling and molecular docking. *Journal of Chromatography A* 2025; **1742**, 465640.

[7] O Babich, S Ivanova, A Bakhtiyarova, O Kalashnikova and S Sukhikh. Medicinal plants are the basis of natural cosmetics. *Process Biochemistry* 2025; **154**, 35-51.

[8] Q Liu, L Sun, Y Zhong, Q Ma and Y Zhuang. Current extraction techniques, biological activities, bioavailability, and patents of rambutan (*Nephelium lappaceum* L.) peel polyphenols: An

updated review. *Trends in Food Science & Technology* 2025; **166**, 105373.

[9] Z Tingting, Z Xiuli, W Kun, S Liping and Z Yongliang. A review: Extraction, phytochemicals, and biological activities of rambutan (*Nephelium lappaceum* L) peel extract. *Heliyon* 2022; **8(11)**, e11314.

[10] JF Osorio-Tobón. Recent advances and comparisons of conventional and alternative extraction techniques of phenolic compounds. *Journal of Food Science and Technology* 2020; **57(12)**, 4299-4315.

[11] E Yulianti, W Warsit, A Sabarudin, B Muchtaromah, IA Putri and SAJN Sholikah. Impact of boiling, ultrasonic, and microwave-ultrasonic assisted extraction on phenolic content, antioxidant activity, and sun protection factor of black tea (*Camellia sinensis*) extracts. *Natural and Life Sciences Communications* 2026; **25(2)**, E2026035.

[12] Y Zhuang, Q Ma, Y Guo and L Sun. Protective effects of rambutan (*Nephelium lappaceum*) peel phenolics on H_2O_2-induced oxidative damages in HepG2 cells and D-galactose induced aging mice. *Food and Chemical Toxicology* 2017; **108**, 554-562.

[13] N Chana, A Muengpoon, S Pethkaew, N Kulsin, A Mahasuk and S Srirat. Screening for phenolic compounds and oxidative capacity of fruit peels, agricultural waste, and traditional herbal medicine for use as biodiesel fuel additive. *Songklanakarin Journal of Science & Technology* 2022; **44(4)**, 1067-1074.

[14] K Boonpisuttinant, R Srisuttee, HY Khong, R Chutoprapat, W Ruksiriwanich, S Udompong, W Chompoo, R Boonbai, R Rakkaew, J Sangsee, K Sriprasert and W Malilas. *In vitro* anti-ageing activities of ethanolic extracts from Pink rambutan (*Nephelium lappaceum* Linn.) for skin applications. *Saudi Pharmaceutical Journal* 2023; **31(4)**, 535-546.

[15] N Lourith, M Kanlayavattanakul, P Chaikul, C Chansriniyom and P Bunwatcharaphansakun. *In vitro* and cellular activities of the selected fruits residues for skin aging treatment. *Anais da Academia Brasileira de Ciências* 2017; **89(S1)**, 577-589.

[16] S Klongdee, W Katekhong, W Jittanit, S Matsukawa and U Klinkesorn. Encapsulation of polyphenol rich extract from rambutan (*Nephelium lappaceum* L.) peel for application as dual functional ingredient in ice cream. *Scientific Reports* 2025; **15(1)**, 30564.

[17] R Meral, Y Erim Kose, Z Ceylan and İ Cavidoglu. The potential use of agro-industrial by-products as sources of bioactive compounds: a nanotechnological approach. *Studies in Natural Products Chemistry* 2022; **73**, 435-466.

[18] JR Nunes, TS Martins and LB Lopes. Nanoemulsions for topical-transdermal administration of a retinoid: understanding the effects of oil phase and terpene concentration on nanoemulsion characteristics, irritation potential, skin penetration and cytotoxicity. *Journal of Drug Delivery Science and Technology* 2025; **113**, 107397.

[19] S Li and Z Zhou. Deciphering the role of endogenous polyphenols in the stability and rheological properties of walnut Oleosome emulsions. *Food Chemistry* 2025; **495**, 146457.

[20] I Lukman, WD Prahastuti, H Herlina, N Chiuman and R Kartasasmita. Insights into molecular interaction of flavonoid compounds in citrus peel bound to collagenase and elastase enzymes: A computational study. *Pharmaceutical Sciences and Research* 2021; **8(2)**, 103-112.

[21] DY Pratiwi, R Saputri, A Nuryanto and N Atikah. Molecular docking study of *Illicium verum* hook f. as elastase and collagenase inhibitor in anti-aging mechanism. *Borneo Journal of Pharmacy* 2025; **8(2)**, 168-177.

[22] U Sukatta, P Rugthaworn, N Khanoonkon, P Anongjanya, K Kongsin, P Sukyai, N Harnkarnsujarit, R Sothornvit and R Chollakup. Rambutan (N*ephelium lappaceum*) peel extract: Antimicrobial and antioxidant activities and its application as a bioactive compound in whey protein isolate film. *Food Packaging and Shelf Life* 2021; **30**, 100735.

[23] S Pedišić, P Čulina, T Pavlešić, N Vahčić, I Elez Garofulić, Z Zorić, V Dragović-Uzelac and M Repajić. Efficiency of microwave- and ultrasound-assisted extraction as a green tool for polyphenolic

isolation from monofloral honeys. *Molecules* 2023; **11(11)**, 3141.

[24] S Siricoon, P Sombatmak, W Sumsakul, T Ploypetchara, W Sorndech, S Butseekhot and C Auranwiwat. Ultrasonic assisted extraction enhanced total phenolic and antioxidant activities from *Aegle marmelos* (L.) Corr. extract. *Journal of Health Science and Alternative Medicine* 2022; **4(3)**, 275-278.

[25] P Kongsune, K Sangthongchin, P Ampha, M Maneechote and N Chana. Enhancement of antioxidant activity and inhibition of polyphenol oxidase from green oak lettuce by chitosan-encapsulated rambutan (*Nephelium lappaceum* L.) peel extract. *Chiang Mai Journal of Science* 2025; **52(4)**, e2025035.

[26] R Re, N Pellegrini, A Proteggente, A Pannala, M Yang and C Rice-Evans. Antioxidant activity applying an improved ABTS radical cation decolorization assay. *Free Radical Biology and Medicine* 1999; **26(9-10)**, 1231-1237.

[27] IF Benzie and JJ Strain. The ferric reducing ability of plasma (FRAP) as a measure of "antioxidant power": The FRAP assay. *Analytical Biochemistry* 1996; **239(1)**, 70-76.

[28] YF Fan, SX Zhu, FB Hou, DF Zhao, QS Pan, YW Xiang, XK Qian, GB Ge and P Wang. Spectrophotometric assays for sensing tyrosinase activity and their applications. *Biosensors* 2021; **11(8)**, 290.

[29] W Wang, Y Gao, W Wang, J Zhang, J Yin, T Le, J Xue, UH Engelhardt and H Jiang. Kojic acid showed consistent inhibitory activity on tyrosinase from mushroom and in cultured B16F10 cells compared with arbutins. *Molecules* 2022; **11(3)**, 502.

[30] B Deri, M Kanteev, M Goldfeder, D Lecina, V Guallar, N Adir and A Fishman. The unravelling of the complex pattern of tyrosinase inhibition. *Scientific Reports* 2016; **6(1)**, 34993.

[31] SH Lee, S Sancheti, S Sancheti and S Seo. Potent antielastase and antityrosinase activities of *Astilbe chinensis*. *American Journal of Pharmacology and Toxicology* 2009; **4(4)**, 127-129.

[32] VL Bodiga and S Bodiga. Ascorbic acid is a potential inhibitor of collagenases-*in silico* and *in vitro* biological studies. *In Silico Drug Design* 2019; **22**, 649-677.

[33] TI Morales and JF Woessner. PZ-peptidase from chick embryos. Purification, properties, and action on collagen peptides. *Journal of Biological Chemistry* 1977; **252(14)**, 4855-4860.

[34] HW Ng, Y Zhang, R Naffa and S Prabakar. Monitoring the degradation of collagen hydrogels by collagenase *clostridium histolyticum*. *Gels* 2020; **6(4)**, 46.

[35] K Bouchemal, S Briancon, E Perrier and H Fessi. Nano-emulsion formulation using spontaneous emulsification: Solvent, oil and surfactant optimisation. *International Journal of Pharmaceutics* 2004; **280**, 241-251.

[36] C Yucel, GS Karatoprak, S Yalcintas and TE Boncu. Ethosomal (-)-epigallocatechin-3-gallate as a novel approach to enhance antioxidant, anti-collagenase and anti-elastase effects. *Beilstein Journal of Nanotechnology* 2022; **13(1)**, 491-502.

[37] G Feinstein, A Kupfer and M Sokolovsky. N-acetyl-(L-Ala) 3-p-nitroanilide as a new chromogenic substrate for elastase. *Biochemical and Biophysical Research Communications* 1973; **50(4)**, 1020-1026.

[38] M Irakli, A Skendi, E Bouloumpasi, P Chatzopoulou and CG Biliaderis. LC-MS identification and quantification of phenolic compounds in solid residues from the essential oil industry. *Antioxidants* 2021; **10(12)**, 2016.

[39] WT Ismaya, HJ Rozeboom, A Weijn, JJ Mes, F Fusetti, HJ Wichers and BW Dijkstra. Crystal structure of *Agaricus bisporus* mushroom tyrosinase: Identity of the tetramer subunits and interaction with tropolone. *Biochemistry* 2011; **50(24)**, 5477-5486.

[40] A Alhayek, AS Abdelsamie, E Schonauer, V Camberlein, E Hutterer, G Posselt, J Serwanja, C Blochl, CG Huber, J Haupenthal, H Brandstetter, S Wessler and AKH Hirsch. Discovery and characterization of synthesized and FDA-approved inhibitors of clostridial and bacillary collagenases. *Journal of Medicinal Chemistry* 2022; **65**, 12933-12955.

[41] C Mattos, DA Giammona, GA Petsko and D Ringe. Structural analysis of the active site of porcine pancreatic elastase based on the X-ray

crystal structures of complexes with trifluoroacetyl-dipeptide-anilide inhibitors. *Biochemistry* 1995; **34(10)**, 3193-3203.

[42] MJ Frisch, M Frisch, G Trucks, K Schlegel, G Scuseria, M Robb, J Cheeseman, J Montgomery, T Vreven, KN Kudin, J Burant, J Millam, S Iyengar, J Tomasi, V Barone, B Mennucci, M Cossi, G Scalmani, N Rega, …, BA Johnson. *Gaussian 03, revision C.02*. Gaussian, Connecticut, United States, 2004.

[43] GM Morris, DS Goodsell, RS Halliday, R Huey, WE Hart, RK Belew and AJ Olson. Automated docking using a Lamarckian genetic algorithm and an empirical binding free energy function. *Journal of Computational Chemistry* 1998; **19(14)**, 1639-1662.

[44] J Stetefeld, SA McKenna and TR Patel. Dynamic light scattering: A practical guide and applications in biomedical sciences. *Biophysical Reviews* 2016; **8(4)**, 409-427.

[45] SD Sarker, L Nahar and Y Kumarasamy. Microtitre plate-based antibacterial assay incorporating resazurin as an indicator of cell growth, and its application in the *in vitro* antibacterial screening of phytochemicals. *Methods* 2007; **42**, 321-324.

[46] A Floegel, DO Kim, SJ Chung, SI Koo and OK Chun. Comparison of ABTS/DPPH assays to measure antioxidant capacity in popular antioxidant-rich US foods. *Journal of Food Composition and Analysis* 2011; **24(7)**, 1043-1048.

[47] B Zou, Y Zhang, R Dai, X Liu and M Zang. Rambutan peel polyphenols improve color and texture of ground pork: Identification, antioxidant and bacteriostatic function, and molecular docking. *LWT* 2025; **220**, 117575.

[48] J Jandaruang, S Phosri, N Poomsuk, S Arthan, S Posoongnoen, T Thummavongsa, K Siriwong and S Preecharram. Bioactivities of leaf extracts from *Urceola polymorpha* (Pierre) D.J.Middleton & Livsh., *Hyptis suaveolens* (L.) Poit, and *Passiflora foetida* L. leaf: Antioxidant, antibacterial, cytotoxic and anti-tyrosinase potential with molecular docking analysis. *Trends in Sciences* 2025; **22(8)**, 10162.

[49] J Xiao, B Liu and Y Zhuang. Effects of rambutan (*Nephelium lappaceum*) peel phenolics and Leu-Ser-Gly Tyr-Gly-Pro on hairless mice skin photoaging induced by ultraviolet irradiation. *Food and Chemical Toxicology* 2019; **129**, 30-37.

[50] CV Ortiz-Ruiz, J Berna, J Tudela, R Varon and F Garcia-Canovas. Action of ellagic acid on the melanin biosynthesis pathway. *Journal of Dermatological Science* 2016; **82(2)**, 115-122.

[51] HL Yang, CP Lin, YV Gowrisankar, PJ Huang, WL Chang, S Shrestha and YC Hseu. The anti-melanogenic effects of ellagic acid through induction of autophagy in melanocytes and suppression of UVA-activated alpha-MSH pathways via Nrf2 activation in keratinocytes. *Biochemical Pharmacology* 2021; **185**, 114454.

[52] M Yoshikawa, H Matsuda, E Harada, T Murakami, N Wariishi, J Yamahara and N Murakami. Elatoside E, a new hypoglycemic principle from the root cortex of *Aralia elata* Seem.: Structure-related hypoglycemic activity of oleanolic acid glycosides. *Chemical and Pharmaceutical Bulletin* 1994; **42(6)**, 1354-1356.

[53] K Jiang, X Zhang, T Li, J Liu, M Liu and S Han. Gibberellin and shikimic acid enhance ascorbic acid accumulation and ROS scavenging ability to delay the senescence of postharvest jujube fruit. *Postharvest Biology and Technology* 2025; **222**, 113340.

[54] D Ren, W Xiong, S Fan, Y Luo, X Jin, F Lai, Z Zhao, R Pei and J Li. Surface functionalization of MXene with gallic acid for enhanced UV aging resistance in SBS-modified asphalt: A study of interface interaction and molecular dynamics. *Colloids and Surfaces A: Physicochemical and Engineering Aspects* 2025; **711**, 136316.

[55] M Bhatiya, S Pathak, G Jothimani, AK Duttaroy and A Banerjee. A comprehensive study on the anti-cancer effects of quercetin and its epigenetic modifications in arresting progression of colon cancer cell proliferation. *Archivum Immunologiae et Therapiae Experimentalis* 2023; **71(1)**, 6.

[56] SA Abdul Ahmad, UD Palanisamy, BA Tejo, MF Chew, HW Tham and SS Hassan. Geraniin extracted from the rind of *Nephelium lappaceum* binds to dengue virus type-2 envelope protein and

inhibits early stage of virus replication. *Virology Journal* 2017; **14(1)**, 229.

[57] S Chan, S Kantham, VM Rao, MK Palanivelu, HL Pham, PN Shaw, RP McGeary and BP Ross. Metal chelation, radical scavenging and inhibition of Abeta42 fibrillation by food constituents in relation to Alzheimer's disease. *Food Chemistry* 2016; **199**, 185-194.

[58] B Iskandar, TW Liu, HC Mei, IC Kuo, MDC Surboyo, HM Lin and CK Lee. Herbal nanoemulsions in cosmetic science: A comprehensive review of design, preparation, formulation, and characterization. *Journal of Food and Drug Analysis* 2024; **32(4)**, 428.

[59] O Sarheed, M Dibi and KV Ramesh. Studies on the effect of oil and surfactant on the formation of alginate-based O/W lidocaine nanocarriers using nanoemulsion template. *Pharmaceutics* 2020; **12(12)**, 1223.

[60] Q Liu, H Huang, H Chen, J Lin and Q Wang. Food-grade nanoemulsions: Preparation, stability and application in encapsulation of bioactive compounds. *Molecules* 2019; **24(23)**, 4242.

[61] T Xiao, B Adhikari, X Ma, Q Wang, H Hu, F Xiang, A Shi and X Zha. Advances in emulsion stability: A review on mechanisms, role of emulsifiers, and applications in food. *Food Chemistry: X* 2025; **29**, 102792.

[62] P Rousta, M Shahamirian, S Yazdanpanah and A Shirazinejad. Co-encapsulation of vitamin D3 and *Cordia myxa* fruit peel extract in nanoemulsions. *British Food Journal* 2025; **127(2)**, 431-450.

[63] BR Albuquerque, J Pinela, MI Dias, C Pereira, J Petrovic, M Sokovic, RC Calhelha, MBPP Oliveira, ICFR Ferreira and L Barros. Valorization of rambutan (*Nephelium lappaceum* L.) peel: Chemical composition, biological activity, and optimized recovery of anthocyanins. *Food Research International* 2023; **165**, 112574.